Estuaries and Coasts (2009) 32:709–719
DOI 10.1007/s12237-009-9162-z

The Role of Kelvin Number on Bulge Formation from Estuarine Buoyant Outflows

Pablo Huq

Received: 10 March 2008 / Revised: 4 February 2009 / Accepted: 12 April 2009 / Published online: 2 May 2009

Abstract This investigation examines the influence of the Kelvin number (K) and fractional depth (h/D) on bulge formation from buoyant outflows from an estuary or strait perpendicular to the coastline. Here $K=W/R$ is the ratio of the width (W) at the mouth of the estuary to the deformation radius (R), and h and D are the buoyant layer and ambient ocean depths, respectively. Measurements of velocity and lateral shear (≈ relative vorticity ζ) at the baymouth are reported for experiments on a flat-bottomed rotating turntable. The form of the velocity profile across the mouth depends on the value of K. The buoyant outflow flows across the entire width of the estuary for narrow estuaries (i.e., $K\leq 1$). In contrast, for wide estuaries ($K>2$), dense oceanic water inflows on the left and the buoyant waters outflow on the right (looking seaward). Velocity profiles of the inflowing oceanic waters are laterally uniform with velocities ($V/C\approx -0.4$), whereas velocity profiles of the outflowing buoyant waters are laterally sheared with peak velocities of $V/C\approx 1.0$ at the right hand exit. The flow pathways when bulges form comprises an anticyclonic turn offshore of the mouth and a downshelf propagating coastal current. Anticyclonic bulges form for surface-advected outflows $h/D<0.25$. Anticyclonic bulges do not form for sufficiently large magnitudes of non-dimensional relative vorticity ζ/f (>0.4), and an additional flow pathway is that buoyant waters recirculate back cyclonically into the estuary at the left-hand (upshelf) side of the estuary. The offshore extent of buoyant waters associated with this cyclonic recirculation can be as large as $7R$.

P. Huq (✉)
College of Marine and Earth Studies, University of Delaware,
Newark, DE 19716, USA
e-mail: huq@udel.edu

Keywords Buoyant outflows · Estuaries · Coastal currents · Bulges

Introduction

Freshwater river outflow is an important component in the dynamics of coastal waters. Such outflows enter the ocean through an estuary or strait and typically form a coastal current. Outflows are laden with silt, sediment, chemicals, agricultural runoff as well as pollution from cities upstream and adversely affect the quality of coastal waters. For example, Wiseman and Kelly (1994) and Rabailais et al. (1996) found that the nitrate-rich plume of the Mississippi River led to anoxia during the summer months. Due to the economic significance of fisheries, the physics of coastal buoyant plumes and its impact on the biology of coastal waters need to be better understood.

Observations have established that a buoyancy-driven coastal current flowing downshelf often forms outside the baymouth. For example, the Delaware Bay outflow persists downshelf for some 200 km from its baymouth (Munchow and Garvine 1993). A second feature of buoyant outflows that sometimes form is a recirculating gyre or bulge. Satellite images show a large bulge (up to 150 km in diameter) that forms at the Tsugaru Strait between Hokkaido and Honshu islands in Japan during the summer and autumn (Sugimoto 1990). Such bulge regions, which are characterized by anticyclonic vorticity, are large in offshore scale relative to the coastal current and can store the majority (~70%) of the river flow exiting to the coastal ocean (Fong and Geyer 2002; Avicola and Huq 2003a, b; Horner-Devine et al. 2006). Thus, the rate at which river water is transported away from the baymouth region depends on whether or not a bulge forms. Bulges have

not been observed for the Delaware Bay or Rhine outflows (Munchow and Garvine 1993; Simpson et al. 1993).

Whether or not bulges form at the baymouth of rivers, or exit of sea straits, is thus crucial for accurate predictions of dispersion of pollution in the coastal ocean. There are also considerable biological implications regarding the fate and transport of crab megalopae and planktonic larvae into and out of estuaries. It has been established that the geometry of the coastline, in particular the radius of curvature of the coastline and the outflow angle of the bay/strait to the coastline, influences whether or not bulges form (Bormans and Garrett 1989; Avicola and Huq 2003a, b; Horner-Devine et al. 2006). The question of how the width of the outflow influences bulge formation requires clarification; the motivation for the present study is to investigate the influence of the Kelvin number, the ratio of estuary width (W) at the baymouth to the internal Rossby radius (R), on bulge formation.

Background

Observational, scaling, and numerical studies have illuminated the characteristics of buoyant outflows. Chao and Boicourt (1986) delineated the presence of a bulge-like region just downstream of the baymouth in their numerical simulations. Garvine (1987) and Munchow and Garvine (1993) found that the structure and dynamics of buoyant plumes depend on the Kelvin number K. The dynamics for $K>1$ are rotational whereas for $K<1$ the influence of the Coriolis force is small. Yankovsky and Chapman (1997) were able to use the ratio of the buoyant layer depth to the total ambient depth (h/D) to classify buoyant plumes as surface, intermediate, or bottom-advected plumes. They also noted that the dynamics of the bulge involved a (cyclostrophic) balance between centrifugal acceleration and pressure gradient and Coriolis force. The unsteady nature of the bulge region that results in its continual growth has been investigated by Nof and Pichevin (2001) and Fong and Geyer (2002). They found that the offshore extent of the bulge was approximately ten times the deformation radius (R) after 10 days. Fong and Geyer also noted dependencies of the geometry of the bulge on the inertial length scale (V/f) and on the width of the baymouth. The dynamics of bulges is susceptible to external effects or forcing. For example, the effect of tides is to stabilize or assist bulge formation (Isobe 2005). Second, bathymetric channels can steer and complicate the development of bulges in buoyant outflows (Masse and Murthy 1992). Third, ambient currents can inhibit bulge formation (Fong and Geyer 2002), or even cause a buoyant outflow to bifurcate and propagate, in both upshelf and downshelf directions (Garcia Berdeal et al. 2002).

The focus of the majority of previous work, both numerical and experimental, has concerned bays equal in width to the deformation radius (i.e., $K=1$). Typically, in these studies, the velocity profile of the buoyant outflow is laterally uniform, and this boundary condition has been termed as the "simple inlet". For example, the numerical simulations of Fong and Geyer (2002) and Narayanan and Garvine (2002) utilized a simple inlet. Similar simple inlets were also utilized in the lab experiments by Kawasaki and Sugimoto (1984) and Horner-Devine et al. (2006). The numerical simulations of Yankovsky (2000) established that an important feature of the simple inlet boundary condition is a cyclonic vortex located on the upshelf side (on the left-hand side looking seaward) of the bay. This allows the possibility of upshelf propagation of buoyant water originating from within the estuary. A numerical examination of inlet conditions was undertaken by Garvine (2001). He divided the outflow into two parts separated by a Margules front and utilized a constant value of across bay velocity gradient $\partial v/\partial x$. Relative to the results with a simple inlet condition, he found that the scales of upshelf intrusion were smaller with a sheared outflow. This shows the importance of the form of the velocity profile in the dynamics of the outflow. In a study of the outflow at the Straits of Gibraltar, Nof (1978) undertook an analysis of the role of vorticity of the buoyant outflow at a wide baymouth over a sill. He found that the presence of lateral shear resulted in deflection of the offshore trajectory of the buoyant plume. An emerging issue in the study of river outflows is the role of the velocity profile at the baymouth. Currently, however, there is a lack of such measurements, and thus a goal of this paper is to report on measurements of baymouth velocity profiles.

The buoyant outflow from wide estuaries was numerically study by Valle-Levinson et al. (1996) for a range of values $2<K<3.6$. They found that rotation produces separation of the buoyant outflow from the left-hand side (looking seaward) of the estuary. This results in dynamical isolation of the outflow and inflow—buoyant outflow occurred on the right hand side (looking seaward) with inflow on the left. A barotropic pressure gradient drives the flow seaward, whereas the baroclinic pressure gradient drives the flow into the bay. Bottom friction slows flows and hinders it from becoming supercritical. The results of the present experiments corroborate the above insights.

Experimental Set-Up

Twenty-three experiments were conducted on a 1.2-m in diameter, flat-bottomed tank and turntable at the Environmental Fluids Laboratory at the University of Delaware. An estuary that is 30 cm long, 15 cm high, and 15 cm

wide is attached to the tank. The width (W) of the estuary was varied between 3.6 cm$<W<$15 cm by the placement of plexiglass inserts. The bottom of the estuary is flush with the bottom of the tank, and the walls of the estuary make a 90° angle, with a sharp radius of curvature, at the coastline (see Figs. 1 and 2). An overhead, co-rotating reservoir of freshwater is the supply for the buoyant outflow which flows through a 1-cm radius pipe located just below the free surface at the end of the bay about 30 cm upstream of the baymouth. The freshwater is mixed with Cole Palmer rhodamine dye to facilitate flow visualization: freshwater flow through the pipe is regulated by a flowmeter. Freshwater flow rates Q_0 were either 6.7 or 10 cm^3/s for which discharge Reynolds numbers were 430 and 650, respectively. Bulge dimensions were determined visually. The tank is filled with brine of a specified density. Following the recommendations of McClimans and Saegrov (1982) for river plume studies with salt stratification, experiments were not undertaken with plume depth h (defined below in Eq. 1) less than 1 cm so as to avoid excessive surface tension and viscous effects. To assess the relative importance of friction for the shallowest ambient water depths, values of the Ekman number $E_K=\upsilon/(fD^2)=(\delta/D)^2$ were calculated. (Here υ is the eddy viscosity; f is the Coriolis parameter; D is the ambient water depth.) The largest values of E_K were $O(10^{-2})$

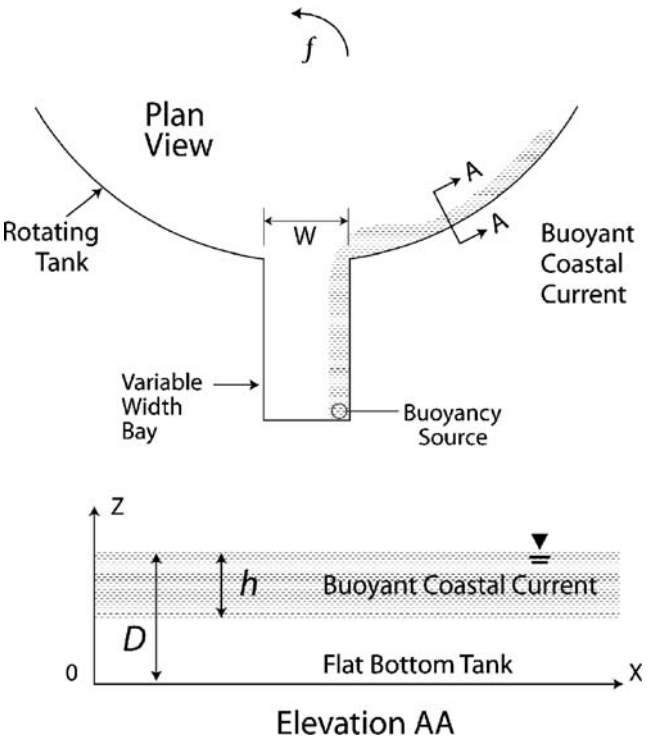

Fig. 1 Plan view of rotating turntable and bay. The width W of the bay is variable. A buoyancy source is located at the upstream end of the bay. The elevation shows that the tank and bay are flat-bottomed. The depths of the buoyant coastal current and total water depth are given by h and D, respectively

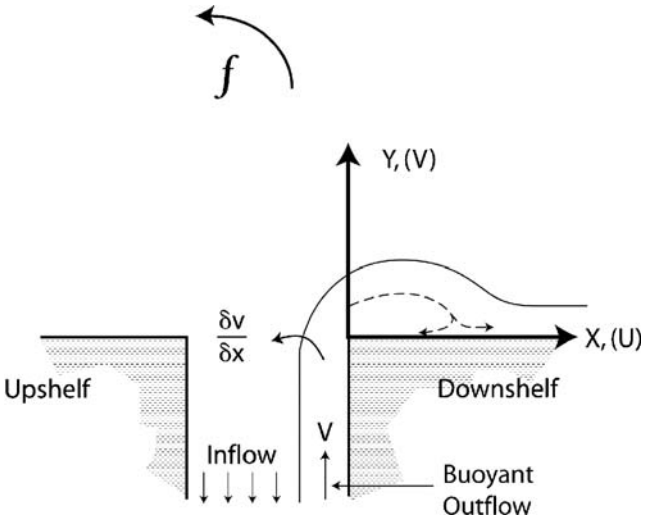

Fig. 2 Coordinate system of the buoyant outflow which flows adjacent to the right hand side of the bay. The offshore direction is y, and the downshelf direction is x. The offshore velocity of the buoyant inflow in the vicinity of the mouth is V. Indicated is the lateral shear $\delta v/\delta x$ across the buoyant outflow at the baymouth

thus the depth of the Ekman layer (δ) was smaller than the ambient water depth (D) even for the smallest depth. Values of E_K were smaller than $O(10^{-3})$ for all depths greater than 2 cm. Thus, viscous effects can be considered to be small in the experiments. Bulge dimensions and rates of growth in experiments with and without surface tension reducing agents were not measurably different. It is known that the eddy viscosity υ varies vertically in the coastal ocean (Lentz 1995) and so frictional effects are considered in terms of the fractional depth h/D rather than the Ekman number E_K which involves a constant eddy viscosity. For $h/D\sim O(0.1)$, the effects of friction are small; in contrast, frictional effects are significant for large fractional depths $h/D\sim O(1)$.

The turntable rotation rate can be set to a desired value to within 0.1 s. Rotation periods ranged between 10.1 and 16.2 s yielding values of Coriolis parameter f of 0.77 s$^{-1}<f<$ 1.25 s^{-1}. The tank is allowed to spin up to solid body rotation for 30 min before experiments were conducted. This is more than twice the time necessary for spin-up for maximum water depths (=8 cm) of the experiments. The magnitude of the surface curvature over the offshore extent of the buoyant waters is small compared to the total depth (approximately 5% for the shallowest depths, and 1% for most runs) and dynamically insignificant for the topographic beta effect to be a first-order effect.

A digital camcorder is suspended above the tank and records the development of the bulge and/or coastal current at 30 Hz. Whole field velocity measurements are obtained through the particle image velocimetry (PIV) technique. The fluid column is seeded with small reflective particles 0.5 mm in diameter. Analysis of consecutive images yielded displacement and velocity vectors. Mean velocities

were resolved to within 10%. Values of reduced gravity g_0' were 4.9 or 14.7 cm/s^2. Densities were measured by hydrometers to within 0.05%. Thermal control and evaporative heat loss are minimized by the use of a plexiglass cover over the tank so that air and water temperatures are maintained to within 0.05°C (the cover also eliminates wind stress.) The rotating turntable is supported by a heavy steel tripod; balance is maintained to within 0.001 radians to eliminate artificial tidal motions.

In order to compare the experimental results to observational and numerical studies, flow parameters must be non-dimensionalized. Vertical, lateral, and velocity scales are non-dimensionalized by the depth scale (h), deformation radius (R), and internal wave speed (C) respectively, where h, R, and C are:

$$h = \sqrt{\frac{2Q_0 f}{g_0'}} \quad R = \frac{\sqrt{g_0' h}}{f} \quad C = \sqrt{g_0' h} \tag{1}$$

Non-dimensional time is t/T, where T is the rotation period of the rotating system. As magnitudes of wind stress and tides are minimal in this study, comparison of the experimental results with oceanic observations is most valid for buoyant outflows under conditions of weak winds and tides. Experimental results are presented in terms of a non-dimensional parameter space comprising Kelvin number $K=W/R$ and also fractional depth h/D. This is done because the Kelvin number discriminates narrow and wide estuaries: estuaries are wide for values of K as small as 2 (Garvine 1995), and dissipation mechanisms such as bottom friction vary with h/D (see scaling analysis below in "Velocity Field at the Mouth/Exit"). Range of values of fractional depth h/D and Kelvin number K varied between $0.14<h/D<1$ and $0.8<K<5.6$. Dimensional values of experimental parameters are given in Table 1 in the Appendix.

Results and Discussion

Results of the presence or absence of a bulge in the parameter space of h/D and K are presented in Fig. 3. An empirical line is drawn to delineate the region of the parameter space favorable to bulge formation. The line extrapolates to the barotropic limit at $K=0$, $h/D=1$. For this limit, the densimetric Froude number $F\sim O(1)$ and the flow are effectively non-rotating and the dynamics are rapid and non-linear (Garvine 1987). The trend for estuaries (up to $K\sim2$) shows that bulge formation occurs with increasing K and deeper oceans (i.e., smaller values of h/D.) It is evident that bulges form for all values of K for small values of $h/D\leq0.25$. That is, bulges form for surface-advected plumes, in agreement with the theory of Yankovsky and Chapman (1997).

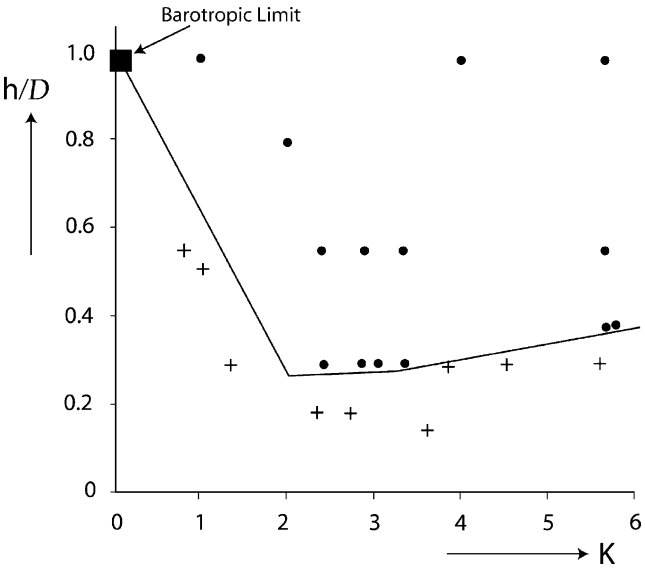

Fig. 3 The experimental results are presented in the parameter space (h/D, K) where h/D is the fractional depth and $K=W/R$, the ratio of the width of the bay to the deformation radius R. *Solid circles* denote the absence of bulges; *plus signs* denote bulges. A *solid line* delineates the parameter space where bulges form—bulges form *below the line*. The *solid square* ($h/D=1$, $K=0$) is the barotropic limit

Bulge Scales

Visualizations and interpretive schematics of the flow field at a time of one revolution period (i.e., $t/T=1$) after the flow reaches the baymouth are shown in Fig. 4. Figure 4a shows the outflow from a narrow bay ($K=0.8$, $h/D=0.55$). The buoyant outflow has formed a circular bulge, and there is a narrow coastal current emerging from the downshelf side of the bulge. However, the flow rate in the coastal current is a small fraction (~20%) of the flow rate at the source at the head of the bay and the volume of freshwater of the coastal current is an order of magnitude smaller than in the bulge (15% and 85%, respectively). The flow within the bulge is anticyclonic. In contrast, the right panel of Fig. 4 shows the flow field for a wide bay ($K\sim5.6$, $h/D=1$). Here a bulge does not form, and the buoyant water, which is transported up to distances 6 or 7R offshore, recirculates back in to the bay. (There is no downshelf coastal current at $t/T\sim1$. Note however that a small-scale downshelf coastal current emerged for $t/T>3$ whose flow rate was less than 5% of the flow rate at the source at the head of the bay.)

The above (cyclonic) recirculation is a new flow pathway for buoyant outflow from estuaries. Previously recognized pathways were the transport via the downshelf coastal current and the storage of buoyant water in the bulge offshore of the mouth of the bay/estuary. At $t/T=1$ the offshore extent (6–7R) of buoyant water associated with the (cyclonic) recirculation is greater than the offshore anticyclonic bulge scales of 2–2.5R for $K=1$ outflows at $t/T=1$

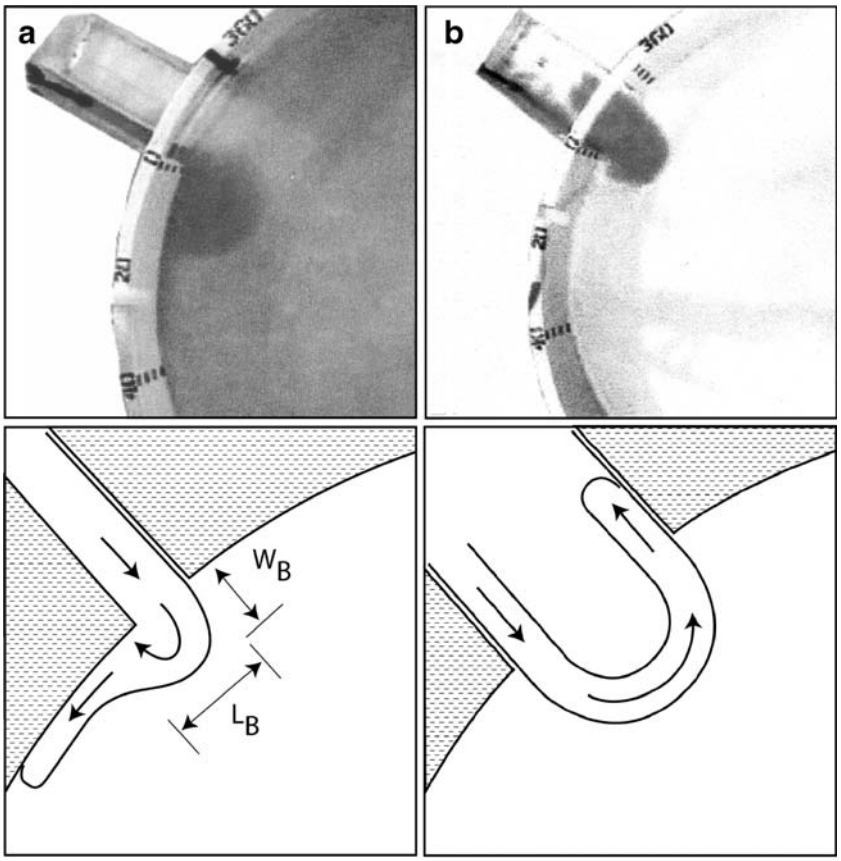

Fig. 4 Visualizations and interpretative schematics. *On the left* (**a**) is a narrow buoyant outflow (K=0.8, h/D=0.55); *on the right* (**b**) is a wide buoyant outflow (K=5.6, h/D=1). The visualizations are for non-dimensional time $t/T \approx 1$. The flow pathway for the narrow outflow comprises an anticyclonic bulge and a buoyant coastal current which propagates downshelf. The flow pathway for the wide outflow differs in that buoyant waters turn cyclonically and recirculate back into the bay: there is no downshelf propagating coastal current. Also shown in the *left-hand schematic* are the length L_B and width W_B of the anticyclonic bulge

determined by Avicola and Huq (2003a, b, see their Fig. 3). The offshore extent is also in agreement with the observational results of Pape and Garvine (1982) for Delaware Bay. Using Woodhead drifters, they found that the region of inflowing water (in to the bay) extended as far offshore as 40 km ($\approx 8R$) offshore from the baymouth.

Observational data of recirculation is rare. To the best of the author's knowledge, the only such data are shown in Fig. 5. This is a 4-day record of the trajectory of two drifters released (within the same tidal cycle) at the seaward edge of the buoyant outflow from Delaware Bay. (Details of the surface drifters drogued at 2 m are given in Munchow and Garvine 1993). The trajectories are suggestive. One of the drifters recirculates back into the bay, whereas the other follows the downshelf coastal current. However, the lack of concurrent salinity measurements prevents a definitive observational demonstration of recirculation. A further point to note is that Fig. 5 suggests that both features of cyclonic eddy which recirculates buoyant water to the bay and a downshelf propagating coastal current can occur or co-exist at the same time. The recognition of a new flow pathway has important consequences for estuary–shelf transport processes. For example, there are implications for the transport of pollution from within to outside the estuary as well as larval recruitment from the ocean.

Details of the evolution of the anticyclonic bulge geometry are given in Fig. 6 for a bay width with non-dimensional parameters K=1.3, h/D=0.28. Bulges form by $t/T \sim 1$. Bulge lengths grow in time to $O(10R)$ by $t/T \sim 3$; widths evolve more slowly to about $5R$ by $t/T \sim 3$. The geometry of the bulge is not circular, rather the bulge aspect ratio (length to width) grows to approximately 2. Bulge scales vary with K. This is shown by comparing the curved

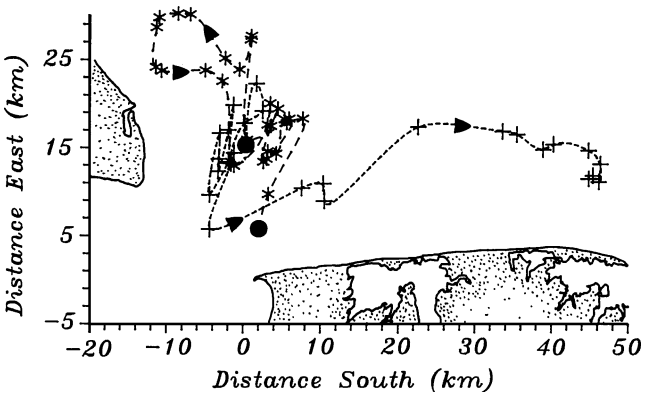

Fig. 5 Observational data of cyclonic recirculation of drifters back into Delaware Bay. The figure shows the trajectories of two drifters (released within the same tidal cycle) for 4 days. One drifter recirculates back into the bay, whereas the other follows the downshelf propagating coastal current. The figure is from Munchow (1992, his Fig. 3.4). For Delaware Bay, the deformation radius $R \sim 6$ km

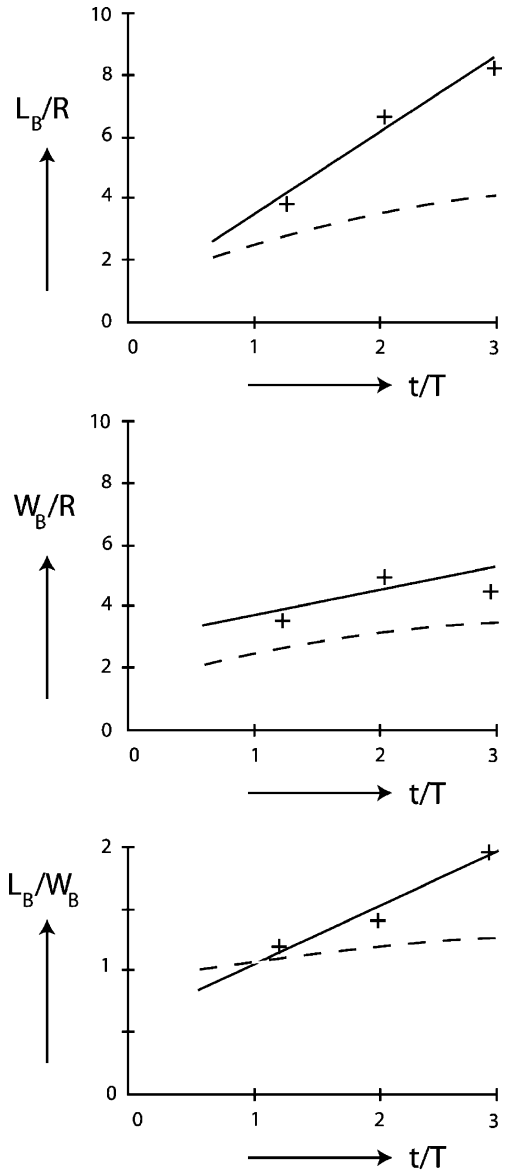

Fig. 6 Graphs of anticyclonic bulge scales as a function of non-dimensional time t/T for a buoyant outflow with K=1.3, h/D=0.28. Shown is the growth of alongshore bulge length L_B, offshore width W_B, and bulge aspect ratio L_B/W_B. The *dashed curved lines* are best-fit trend lines for bulge evolution for K=1, h/D≈0.2–0.3 outflows of Avicola and Huq (2003a, b)

trend lines of the K=1 outflow (Avicola and Huq 2003a, b) which are also drawn in Fig. 6. As K increases from 1 to 1.3, it is evident that the length of the bulge changes more than the width, and also that the aspect ratio of the bulge of the K=1 outflow is smaller (i.e., more circular). These trends are similar to the numerical results of Fong and Geyer (2002); they found that the aspect ratio of the bulge for their K=1 outflows is more circular for high Rossby number R_O outflows $\left(R_O = \frac{V}{fR}\right)$ than for low Rossby number outflows. They also noted that "the alongshore extent of the bulge is related to the width of the river mouth" (p. 964). Utilizing the width W of the estuary in the denominator of R_O yields a modified Rossby number $R_O' = \frac{V}{fRK}$ that is useful in the scaling of the bulge geometry. Aspect ratios of bulges are less circular for a high Rossby number outflow for a wide outflow (i.e., K >1) than for the same high Rossby number outflow from a narrower outflow, as the value of R_O' is smaller for the wide outflow.

Velocity Field at the Mouth/Exit

Observations of bulge formation in the parameter space (h/D, K) of Fig. 3 shows that bulges formed for K<2 and K>3.5 but do not form for 2<K<3.5 for values of fractional depth h/D~0.25. Thus, we focus on velocity data along a transect h/D~0.25 for various values of K. The form or profile of the velocity field at the baymouth depends on the value of K (see Fig. 7). For narrow bays (K~1.3), velocity is greatest (V/C~0.5) near the right hand coast (at x/R~−0.25). Magnitude of non-dimensional shear $(\Delta V/C)/(\Delta x/R)$ is about 0.2. Visual observations showed that the inflow into the bay occurs under the outflow so that there is a two-layer structure at the baymouth.

For wider bays (K~3.5) maximum velocities at the right-hand coast increase to V/C=0.9. Inflow to the bay with velocities V/C=−0.4 occur on the left-hand side of the bay from $-2 \le x/R \le -3.5$: the inflowing velocity profile is uniform laterally. (Integration of velocity profiles showed that magnitudes of inflow and outflow were equal.) Similar outflow and inflow velocity profiles arise for even wider bays (K~5.6). Generally, the trend for outflow velocities of the buoyant outflow is that maximum velocities occur at the right hand side and approach critical values (V/C≈1) for wide bays. Another characteristic feature of buoyant outflows from wide bays is the strongly laterally sheared region between the inflow and the outflow: velocity differences of about V/C=0.7 occur over transverse distances as small as $0.25x/R$. Note that lateral shear $\frac{\partial V}{\partial x}$ is approximately equal to the vertical component of relative vorticity $\zeta = \left(\frac{\partial V}{\partial x} - \frac{\partial U}{\partial y}\right)$ as $\frac{\partial U}{\partial y}$ is relatively small. Thus, lateral shear $\frac{\partial V}{\partial x}$ results in cyclonic rotation of the outflow; this influences bulge formation as discussed below.

Experimental data for the widths of the buoyant outflow and inflow at the baymouth, defined by the location of zero velocity for V/C, varies with K (see Fig. 8). Note that the widths are scaled by the deformation radius R. Inflows occur for bays with K>1.3. Also shown (open symbols) in Fig. 8 are the widths of buoyant outflow and dense inflow for wide, shallow bays (K=5.6, h/D=1). For h/D~1, outflow and inflow widths (x/R~1.8) are smaller than the widths (x/R~2.8, 2.5, respectively) for deep bays (h/D~0.25). The effect of bottom friction is to attenuate the lateral or transverse scales of outflow and inflow. Observations for Delaware Bay (K~3.5, h/D~1) show that the width of

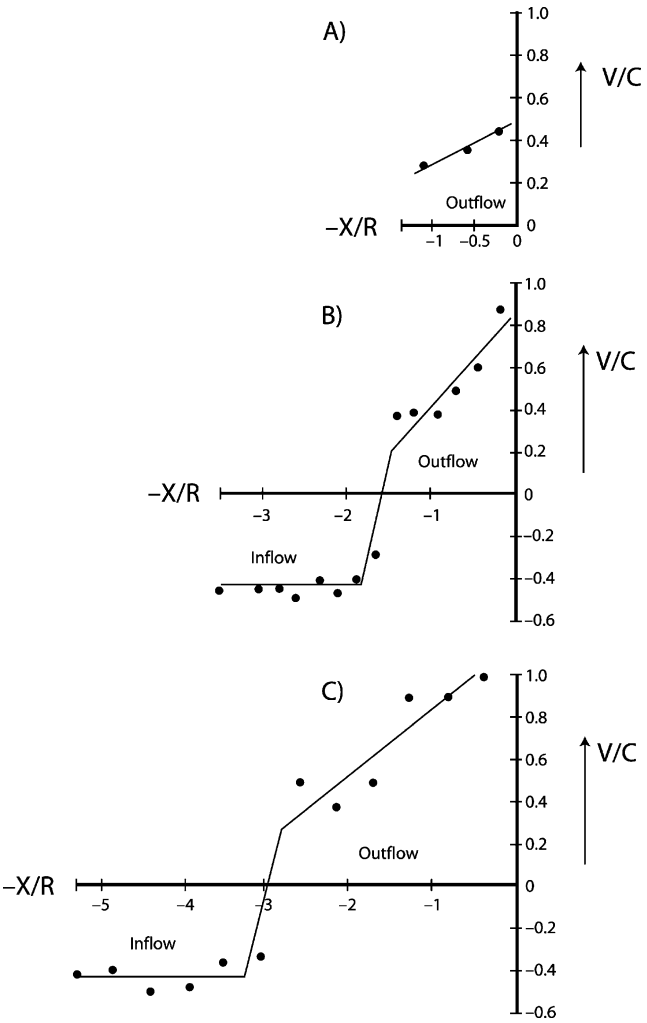

Fig. 7 **a**–**c** Measurements of non-dimensional velocity V/C across the baymouth for three different buoyant outflows (K=1.3, h/D=0.28; K=3.5, h/D=0.14; K=5.6, h/D=0.28). The peak velocity of the buoyant outflow V/C adjacent to the right hand coast increases with K, and the lateral (across-shore) velocity profile of the buoyant outflow is also increasingly sheared. The velocity profile of the inflow is uniform. Velocities measured for times up to t/T~3

buoyant outflow at the mouth is ~7 km and R~5 km (Munchow and Garvine 1993). This gives $-X/R$=1.4 which is in excellent accord with the present data.

Bulge formation depends on the outcome of the competition between the lateral shear, which turns the buoyant outflow cyclonically, and the anticyclonic rotation of inertial response of (V/f) as the buoyant outflow exits the baymouth. The sense of rotation of lateral shear at the baymouth augments planetary vorticity (f). For sufficiently large values of absolute vorticity (ζ+f), bulges do not form, as the tendency to turn cyclonically is greater than the anticyclonic trajectories (with inertial radius ~V/f). Measurements of non-dimensional relative vorticity ζ/f at the baymouth, presented in Fig. 9, indicate that values of ζ/f increases to about 0.4 with increasing values of K. In Fig. 9,

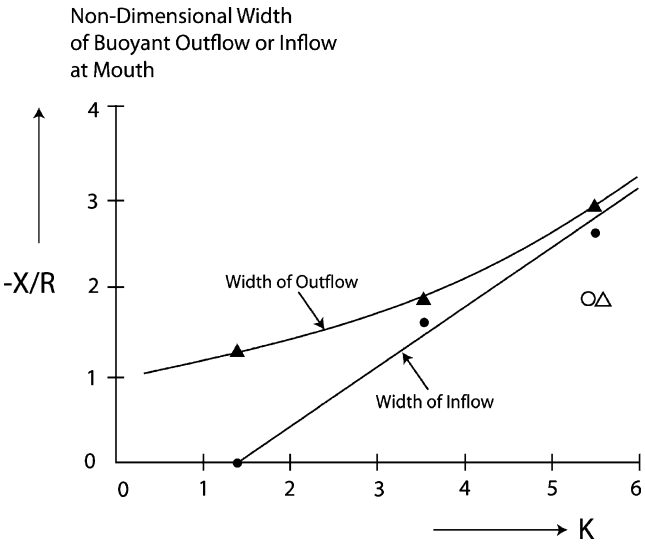

Fig. 8 Graph of non-dimensional width of buoyant outflow and inflow at the baymouth as a function of Kelvin number K. The buoyant outflow is deflected to the right by the Coriolis force and separates from the left-hand coast for bays wider than K>1.3. For the *solid symbols*, the experimental parameters are the same (i.e., 1.3<K<5.6, h/D~0.25) as in the caption for Fig. 7. The *open symbols* indicate that the scales of the inflow and outflow are smaller for large fractional depth (h/D~1)

bulges formed for K=1.3 and 3.5 outflows. K=5.6 outflows are marginal as regards bulge formation; bulges did not form for h/D~0.4 outflows but did form for h/D~0.28 outflows (see Fig. 3). Also shown in Fig. 9 are field data for ζ/f for Delaware Bay and Hudson River outflows (Munchow and Garvine 1993; Chant et al. 2008, respectively.) Bulges have been observed for the Hudson River but not for Delaware Bay outflow. In conjunction, the lab and field

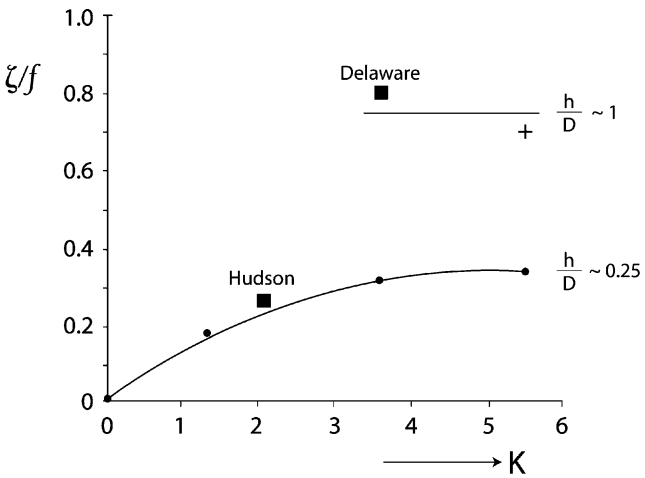

Fig. 9 Graph of the variation of lateral shear or non-dimensional relative vorticity ζ/f at the baymouth with Kelvin number K. *Solid circles* are data for K=1.3, 3.5, and 5.6 and h/D~0.25 buoyant outflows (see caption for Fig. 7). The *plus symbol* is data for large fractional depth h/D~1. Data for Delaware Bay and Hudson River are denoted by the *solid squares*

data suggest that bulges occur for $\zeta/f<0.4$. The value of relative vorticity ζ/f for $K=5.6$, $h/D\sim1$ shallow buoyant outflow is also plotted in Fig. 9. Comparison with values of ζ/f for deep ($h/D\sim0.25$) outflows reveals that the proximity of the bottom (i.e., bottom friction) increases the magnitude of relative vorticity.

The relative magnitudes of ζ and f are also useful in assessing the dynamics. Non-linear inertial accelerations are relatively unimportant in the momentum balance if ζ is much smaller than f (Pedlosky 1978). Thus, as the value of the non-dimensional ratio ζ/f approaches $O(1)$, it can be deduced that the momentum balance at the baymouth is increasingly non-linear. Scaling analysis provides insights on the magnitudes of the relative contributions from non-linear advection, Coriolis force, pressure gradient, and friction. Figure 2 shows the coordinate system (y and V) are the coordinate and depth averaged velocity of the buoyant layer along the longitudinal axis of the bay; x and U are the coordinate and depth averaged velocity laterally across the baymouth. Time derivatives and wind stress are neglected in the scaling analysis as the experiments are undertaken with a steady-state source and wind stress is zero. Consider the momentum balance along the y-direction (i.e., along the longitudinal axis of the bay).

$$V\frac{\partial V}{\partial y}+U\frac{\partial V}{\partial x}+fU=-\frac{1}{\rho_0}\frac{\partial P}{\partial y}-\frac{\tau_b}{\rho_0 h} \tag{2a}$$

$$\frac{V^2}{fUL_y} \quad \frac{V}{fL_x} \quad 1 \quad \frac{g'h}{fUL_y} \quad \frac{rV}{hfU} \tag{2b}$$

$$\frac{R_O}{\gamma^2} \quad \frac{R_O}{\gamma^2} \quad 1 \quad \frac{1}{K^2R_O} \quad \frac{1}{\gamma}\frac{r}{fh} \tag{2c}$$

$$\begin{array}{lllll} O(1) & O(1) & 1 & O(1) & O(10^{-1}) \quad h/D\sim1,\ K\sim1 \\ O(1) & O(1) & 1 & O(1) & O(10^{-2}) \quad h/D\sim0.1,\ K\sim1 \\ O(1) & O(1) & 1 & O(1) & O(10^{-1}) \quad h/D\sim1,\ K>1 \\ O(0.1-1) & O(0.1-1) & 1 & O(1) & O(10^{-3}) \quad h/D\sim0.1,\ K>1 \end{array} \tag{2d}$$

Order of magnitude estimates for each term are given in Eq. 2b. The baroclinic pressure gradient term $\frac{1}{\rho_0}\frac{\partial P}{\partial y}$ is estimated as $\frac{gh}{\rho_0}\frac{\partial \rho}{\partial y}$. Frictional losses are represented by $\tau_b=r\rho V$. Estimates in terms of non-dimensional parameters $R_O\sim\frac{U}{fL_y}\sim\frac{\gamma^2V}{fL_x}$ and Kelvin number $K=W/R$ and the ratio $\gamma=\frac{U}{V}$ of across-shore velocity U to along shore velocity V are given in Eq. 2c. Measured values (see Table 1 in the Appendix and figures) from the experiments are used to estimate the magnitudes of the terms in Eq. 2d for the cases of narrow ($K\sim1$) and wide ($K>1$), and deep $h/D=O(0.1)$ and shallow $h/D=O(1)$ geometry of estuaries. Values of the friction coefficient r were $r=0.01$ cm/s and 0.001 cm/s for $h/D=O(1)$ and $h/D=O(0.1)$, respectively. Typical values used were $V=2$ cm/s; $L_x=4$ cm; $h=2$ cm; Coriolis parameter $f=1$ s^{-1}; ρ_0 is the averaged coastal water density; and g' is reduced gravity. The longitudinal length scale (L_y) is estimated from the equation of continuity as $L_y=O(L_xV/U)$. Observations show that typical values of the ratio γ were $O(10^{-2})$; an exception is values γ of $O(10^{-1})$ for wide, deep buoyant outflows (i.e., $K>1$, $h/D=O(0.1)$). Values of the frictional term $\frac{1}{\gamma}\frac{r}{fh}$ were of $O(10^{-1})$ and $O(10^{-2}$ or $10^{-3})$ for $h/D=O(0.1)$ and $h/D=O(1)$, respectively.

The dynamical balances involve significant contributions from non-linear advection, Coriolis, and pressure gradient terms for all cases; it is evident that the role of friction is the principal difference between the cases. Examination of the parameterized frictional term $\frac{1}{\gamma}\frac{r}{fh}$ shows that the depth of the estuary is a principal factor determining the magnitude of friction. For shallow ($h/D\sim1$) estuaries, values of $\frac{1}{\gamma}\frac{r}{fh}\sim O(10^{-1})$, whereas for deep ($h/D\sim0.1$) estuaries, values are smaller $\frac{1}{\gamma}\frac{r}{fh}\sim O(10^{-2}$ or $10^{-3})$; friction attendant with shallow ambient depths constrains lateral or transverse scales of the exiting buoyant outflow (compare open and solid symbols in Fig. 8). The consequence of this is greater transverse velocity gradients $\frac{\partial V}{\partial x}$ and relative vorticity $\zeta\sim\frac{\partial V}{\partial x}$ (see Fig. 9).

The role of width variations is clarified by scaling analysis; the presence of the Kelvin number in the denominator of the scaled longitudinal pressure gradient term in Eq. 2c indicates that the relative contribution of the longitudinal pressure gradient diminishes for wide outflows ($K>1$). Offsetting this will be greater non-linear advection. Wide estuaries have room to allow the buoyant plume to expand or adjust. Measurements show that transverse adjustment occurs when frictional effects are small (i.e., for deep outflows $h/D\sim O(10^{-1})$), and for such cases, values of the velocity ratio γ increase to $O(10^{-1})$. For shallow wide outflows (i.e., $K>1$, $h/D=O(1)$), friction inhibits transverse adjustment and values of $\gamma\sim O(10^{-2})$. The outflow does not adjust for narrow outflows ($K\sim1$) and values of γ are also of $O(10^{-2})$. To reiterate, increasing friction attenuates transverse scales and increases transverse velocity gradients; in contrast, increasing outflow width allows expansion and decreases transverse gradients. This competition is reflected in the experimental parameter space (h/D, K).

The present experimental results are in accord with the conclusions of the numerical studies of density-driven estuarine outflows of Valle-Levinson (2008). He explored patterns of flow as a function of width, friction, and rotation. For weak friction, the outflow is laterally sheared for large K and vertically sheared for small K. For moderate friction, the outflow is both horizontally and vertically sheared: for strong friction the outflow is laterally sheared.

A schematic of the trends in the parameter space (h/D, K) is presented as Fig. 10. For small values of K (~1), the buoyant outflow lacks space to spread laterally. Conversely

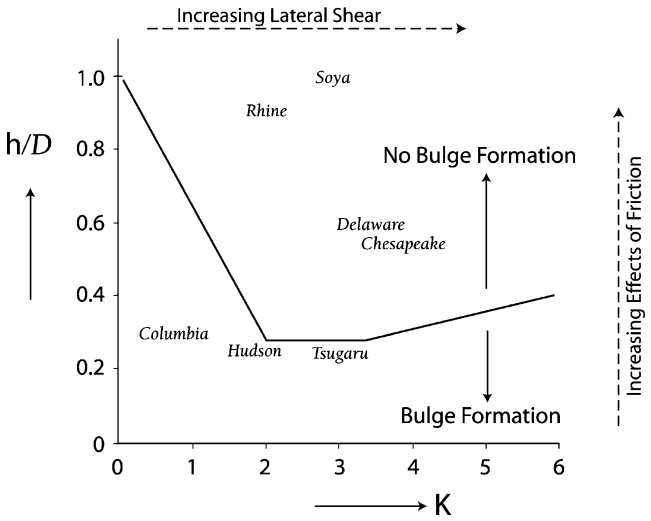

Fig. 10 Observational data of bulge formation in the experimental parameter space (h/D, K). Lateral shear increases with increasing values of Kelvin number K. Effects of friction increase with increasing fractional depth h/D. Bulges form for sufficiently deep oceans. The *solid line* determined from experimental data delineates bulge formation (see Fig. 3). Various different buoyant outflows are located in the parameter space by their respective values of h/D and K. Anticyclonic bulges have only been observed for the Columbia, Hudson, and Tsugaru outflows

for wide bays ($K>2$), the buoyant outflow adjusts so that the outflow is wide and laterally sheared. The effects of turbulence generated by bottom friction, which results in vertical and lateral mixing of mass and momentum, depend on the fractional depth h/D. The likelihood of bulge formation becomes independent of h/D for a sufficiently deep ocean as bottom friction no longer plays a significant role in the dynamical balances. It is hoped that the present results will encourage observational studies. Further numerical simulations of buoyant outflows, inside and outside the bay, would be useful in evaluating terms such as barotropic and baroclinic pressure gradients that are difficult to resolve experimentally.

Comparison with Field Observations

Field observations of bulge formation in the parameter space (h/D, K) are presented in Fig. 10. Bulges have not been observed for the Chesapeake, Delaware, Rhine, and Soya outflows: the parameters of these outflows lie above the empirical dividing line in the parameter space (h/D, K) for bulge formation. Bulges have been observed for the Columbia (Hickey et al. 1998), Hudson (Chant et al. 2008), and Tsugaru outflows (Sugimoto 1990)—the parameters of which fall below the dividing line. It is evident that lab data and observations of bulge formation are in excellent agreement.

Figure 10 also usefully indicates that the dynamics of the Hudson and Tsugaru outflows are marginal with regard to bulge formation as their parameters lie close to the dividing line. The implication is that they will be susceptible to other factors such as wind, magnitude of discharge, and ambient stratification. For example, winds can augment freshwater storage within the bay and so affect flow rates exiting through the baymouth (Janzen and Wong 2002). Of course, outside the bay, winds influence the mixing and transport and alter the vertical structure of buoyant outflows (Whitney and Garvine 2005; Lentz and Largier 2006). Indeed, Choi and Wilkin (2007) determined that winds blowing to the north suppressed bulge formation for the Hudson outflow. The Tsugaru outflow forms bulges during the summer and autumn when flow rates are large; Kawasaki and Sugimoto (1984) remark that the local mixed layer depth is likely to be a significant factor in inhibiting bulge formation in the winter and spring.

Conclusions

Bulge formation from buoyant outflows exiting from the mouth of an estuary/bay/strait perpendicular to the coastline is investigated in experiments undertaken on a flat-bottomed rotating turntable experiments. In particular, the influences of variations of width and flow depth at the exit or mouth are investigated. Results are presented in the parameter space (h/D, K) where h/D is the fractional depth, and K is the Kelvin number, the non-dimensional width of the exit or mouth. The ordinate h/D reflects the role of the effects of bottom friction, whereas the abscissa K reflects the effects of lateral shear. Measurements at the baymouth show that the value of non-dimensional relative vorticity ζ/f (approximately equal to lateral shear) increases with increasing values of K and h/D. Sufficiently large values of ζ/f inhibit bulge formation. Bulges formed for surface-advected flows where $h/D<0.25$. The data of Fig. 3 show that the delineation between bulge formation or its absence varied with both parameters h/D and K as $h/D \rightarrow O(1)$.

The form of the velocity profile at the mouth varies with the Kelvin number K. For $K\approx1$ outflows, buoyant waters flow out over the entire width, and inflow of dense oceanic water occurs under the buoyant outflow. For $K>1.3$, the buoyant outflow is deflected to the right by the action of the Coriolis force and detaches from the left-hand (upshelf) coast; for such cases, inflow of dense oceanic water occurs on the left-hand side of the mouth and buoyant outflow on the right. For very wide mouths ($K>3.5$), the transverse scales (or widths) of the inflow and outflow are similar. Velocities of the buoyant outflow also vary with K. For $K\approx1$ outflows, peak velocities are $V/C\approx0.5$; for very wide bays ($K>3.5$), peak values of outflow velocity approach critical values $V/C\approx1$ immediately adjacent to the right hand side coast and the velocity profile of the

buoyant outflow across the mouth is laterally sheared. Measurements show that relative vorticity ζ/f increases to values of about 0.4 with increasing K for $h/D \sim 0.25$; values of ζ/f increase to 0.7–0.8 for large fractional depths $h/D \sim 1$ (see Fig. 9).

When bulges form, then, the trajectory or the pathway of buoyant waters comprises an anticyclonic turn offshore of the mouth and a coastal current propagating downshelf. If the absolute vorticity ($f+\zeta$) at the mouth is sufficiently large (>1.4), then anticyclonic bulges do not form, rather the buoyant waters turn cyclonically and return into the mouth at the left-hand side. The offshore extent of buoyant waters associated with this cyclonic rotation can be large in scale (~7R). This recirculation of buoyant waters back into the bay or estuary has important consequences for biological pathways and transport of pollution. For example, it is likely that the residence time of an estuary/bay will increase with increasing magnitudes of recirculation.

Acknowledgment The collegiality of Rich Garvine is greatly missed: this paper is dedicated to him.

Appendix

Q_O	T	g_0'	W	D	C	R	h/D	K
cm^3/s	s	cm s^{-2}	cm	cm	cm/s	cm	–	–
10	13.1	14.7	15	8	4.1	4.3	0.14	3.5
10	10.1	4.9	3.6	8	3.3	2.7	0.28	1.3
10	10.1	4.9	10	8	3.3	2.7	0.28	3.8
10	10.1	4.9	12	8	3.3	2.7	0.28	4.5
10	10.1	4.9	15	8	3.3	2.7	0.28	5.6
10	10.2	4.9	15	2	3.3	2.7	1	5.6
10	14	14.7	15	2	4	4.5	0.55	3.3
10	14	14.7	3.6	2	4	4.5	0.55	0.8
10	14	14.7	10.5	2	4	4.5	0.55	2.3
10	14	14.7	12.2	2	4	4.5	0.55	2.7
10	14	14.7	10.5	4	4	4.5	0.28	2.3
10	14	14.7	15	4	4	4.5	0.28	3.3
10	10.1	4.9	15	4	3.3	2.7	0.56	5.6
10	14	14.7	10.5	6	4	4.5	0.18	2.3
10	14	14.7	12.2	6	4	4.5	0.18	2.7
10	14	14.7	12.2	4	4	4.5	0.28	2.7
10	10	4.9	15	6	3.3	2.7	0.38	5.7
10	16.2	14.7	5	1	3.9	5	1	1
10	16.2	14.7	5	2	3.9	5	0.5	1
6.7	13.4	4.9	6	2	2.8	3	0.8	2
6.7	12	14.7	12	4	4.2	4	0.3	3
6.7	11.8	4.9	12	2	3.2	3	1	4
10	10.1	4.9	15	6	3.3	2.7	0.38	5.6

References

Avicola, G., and P. Huq. 2003a. The characteristics of the recirculating bulge region in coastal buoyant outflows. *Journal of Marine Research* 61: 435–463. doi:10.1357/002224003322384889.

Avicola, G., and P. Huq. 2003b. The role of outflow geometry in the formation of the recirculating bulge region in coastal buoyant outflows. *Journal of Marine Research* 61: 411–434. doi:10.1357/002224003322384870.

Bormans, M., and C. Garrett. 1989. A simple criterion for gyre formation by the surface outflow from a strait, with application to the Alboran Sea. *Journal of Geophysical Research* 94(C9): 12637–12644. doi:10.1029/JC094iC09p12637.

Chant, R.J., S.M. Glenn, E. Hunter, J. Kohut, R.F. Chen, R.W. Houghton, J. Bosch, and O. Schofield. 2008. Bulge formation of a buoyant river plume. *Journal of Geophysical Research* 113: C01017. doi:10.1029/2007JC004100.

Chao, S.-Y., and W.C. Boicourt. 1986. Onset of estuarine plumes. *Journal of Physical Oceanography* 16: 2137–2149. doi:10.1175/1520-0485(1986)016<2137:OOEP>2.0.CO;2.

Choi, B.-J., and J.L. Wilkin. 2007. The effect of wind on the dispersal of the Hudson River plume. *Journal of Physical Oceanography* 37: 1878–1897.

Fong, D.A., and W.R. Geyer. 2002. The alongshore transport of freshwater in a surface trapped river plume. *Journal of Physical Oceanography* 32: 957–972. doi:10.1175/1520-0485(2002)032<0957:TATOFI>2.0.CO;2.

Garvine, R.W. 2001. The impact of model configuration in studies of buoyant coastal discharge. *Journal of Marine Research* 59: 193–225. doi:10.1357/002224001762882637.

Garvine, R.W. 1995. A dynamical system of classifying buoyant coastal discharges. *Continental Shelf Research* 15: 1585–1596. doi:10.1016/0278-4343(94)00065-U.

Garvine, R.W. 1987. Estuary plumes and fronts in shelf waters: a layer model. *Journal of Physical Oceanography* 11: 1877–1895. doi:10.1175/1520-0485(1987)017<1877:EPAFIS>2.0.CO;2.

Garcia Berdeal, I., B.M. Hickey, and M. Kawase. 2002. Influence of wind stress and ambient flow on a high discharge river plume. *Journal of Geophysical Research* 107(C9): 3103. doi:10.1029/2001JC000932.

Hickey, B.M., L.J. Pietrafesa, D.A. Jay, and W.C. Boicourt. 1998. The Columbia River Plume Study: subtidal variability in the velocity and salinity fields. *Journal of Geophysical Research* 103: 10339–10368. doi:10.1029/97JC03290.

Horner-Devine, A., D. Fong, S. Monismith, and T. Maxworthy. 2006. Laboratory experiments simulating a coastal river inflow. *Journal of Fluid Mechanics* 555: 203–232. doi:10.1017/S0022112006008937.

Isobe, A. 2005. Ballooning of River-Plume Bulge and its stabilization by tidal currents. *Journal of Physical Oceanography* 35: 2337–2351. doi:10.1175/JPO2837.1.

Janzen, C.D., and K.-C. Wong. 2002. Wind forced dynamics at the estuary-shelf interface of a large coastal plain estuary. *Journal of Geophysical Research* 107: 3138. doi:10.1029/2001JC000959.

Kawasaki, Y. and T. Sugimoto, 1984: Experimental studies on the formation and degeneration process of the Tsugaru Warm Gyre. In *Ocean Hydrodynamics of the Japan and East China Seas*, ed. T. Ichiye, 225-238. Oceanog. Series. No. 39, Elsevier.

Lentz, S.J., and J. Largier. 2006. The influence of wind forcing on the Chesapeake Bay Buoyant Coastal Current. *Journal of Physical Oceanography* 36: 1305–1316. doi:10.1175/JPO2909.1.

Lentz, S.J. 1995. Sensitivity of the inner-shelf circulation to the form of the eddy viscosity profile. *Journal of Physical Oceanography* 25: 19–28. doi:10.1175/1520-0485(1995)025<0019:SOTISC>2.0.CO;2.

McClimans, T.A., and S. Saegrov. 1982. River plume studies in distorted Froude Models. *Journal of Hydraulic Research* 20(1): 15–27.

Masse, A.K., and C.R. Murthy. 1992. Analysis of the Niagara River plume dynamics. *Journal of Geophysical Research* 97: 2403–2420. doi:10.1029/91JC02726.

Munchow, A. 1992. The formation of a buoyancy driven coastal current, PhD thesis, Univ. of Delaware, 205 pp.

Munchow, A., and R.W. Garvine. 1993. Dynamical properties of a buoyancy-driven coastal current. *Journal of Geophysical Research* 98: 20063–20077. doi:10.1029/93JC02112.

Narayanan, C., and R.W. Garvine. 2002. Large-scale buoyancy driven circulation on the continental shelf. *Dynamic of Atmospheric Oceans* 36: 125–152. doi:10.1016/S0377-0265(02)00028-3.

Nof, D. 1978. On geostrophic adjustment in sea straits and wide estuaries: theory and lab experiments. Part 2-two layer system. *Journal of Physical Oceanography* 8(5): 861–872. doi:10.1175/1520-0485(1978)008<0861:OGAISS>2.0.CO;2.

Nof, D., and T. Pichevin. 2001. The ballooning of outflows. *Journal of Physical Oceanography* 31: 3045–3058. doi:10.1175/1520-0485(2001)031<3045:TBOO>2.0.CO;2.

Pape, E.H., and R.W. Garvine. 1982. The subtidal circulation in Delaware Bay and adjacent shelf waters. *Journal of Geophysical Research* 87: 7955–7970. doi:10.1029/JC087iC10p07955.

Pedlosky, J. 1978. Geophysical fluid dynamics. Springer-Verlag, 710 pp.

Rabailais, N.N., R.E. Turner, D. Justic, Q. Dortch, W.J. Wiseman, and B.K. Sen Gupta. 1996. Nutrient changes in the Mississippi River and system responses on the adjacent continental shelf. *Estuaries* 19: 386–407. doi:10.2307/1352458.

Simpson, J.H., W.G. Bos, F. Schirmer, A.J. Souja, T.P. Rippeth, S.E. Jones, and D. Hydes. 1993. *Oceanologica Acta* 16(1): 23–32.

Sugimoto, T. 1990. A review of recent physical investigations on the straits around the Japanese Islands. In *The Physical Oceanography of Sea Straits*, ed. L.J. Pratt, 191–209. Amsterdam: Kluwer.

Valle-Levinson, A. 2008. Density-driven exchange flow in terms of the Kelvin and Ekman numbers. *Journal of Geophysical Research* 113: C04001. doi:10:1029/2007JC004144.

Valle-Levinson, A., J.M. Klinck, and G.H. Wheless. 1996. Inflows/outflows at the transition between a coastal plain estuary and the coastal ocean. *Continental Shelf Research* 16: 1819–1847. doi:10.1016/0278-4343(96)00016-7.

Whitney, M.M., and R.W. Garvine. 2005. Wind influences on a coastal buoyant outflow. *Journal of Geophysical Research* 110. doi:10.1029/2003jc002261.

Wiseman, W.J., and F.J. Kelly. 1994. Salinity variability within the Louisiana coastal current during the 1982 flood season. *Estuaries* 17(4): 732–739. doi:10.2307/1352743.

Yankovsky, A.E. 2000. The cyclonic turning and propagation of buoyant coastal discharge along the shelf. *Journal of Marine Research* 58: 585–607. doi:10.1357/002224000321511034.

Yankovsky, A.E., and D.C. Chapman. 1997. A simple theory for the fate of buoyant coastal discharges. *Journal of Physical oceanography* 27: 1386–1401. doi:10.1175/1520-0485(1997)027<1386:ASTFTF>2.0.CO;2.